

Acoustic monitoring of gas emissions from the seafloor. Part II: a case study from the Sea of Marmara

Gaye Bayrakci, Carla Scalabrin, Stéphanie Dupré, Isabelle Leblond, Jean-Baptiste Tary, Nadine Lanteri, Jean-Marie Augustin, et al.

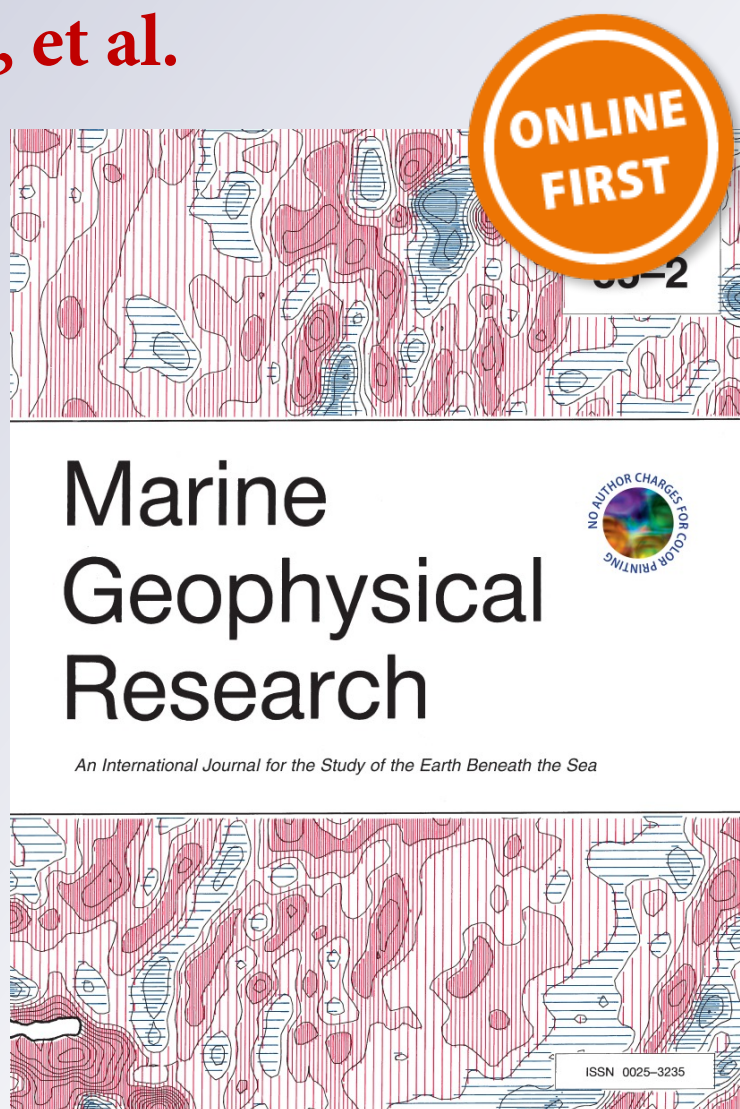
Marine Geophysical Research

An International Journal for the Study of the Earth Beneath the Sea

ISSN 0025-3235

Mar Geophys Res

DOI 10.1007/s11001-014-9227-7



Your article is protected by copyright and all rights are held exclusively by Springer Science +Business Media Dordrecht. This e-offprint is for personal use only and shall not be self-archived in electronic repositories. If you wish to self-archive your article, please use the accepted manuscript version for posting on your own website. You may further deposit the accepted manuscript version in any repository, provided it is only made publicly available 12 months after official publication or later and provided acknowledgement is given to the original source of publication and a link is inserted to the published article on Springer's website. The link must be accompanied by the following text: "The final publication is available at link.springer.com".

Acoustic monitoring of gas emissions from the seafloor. Part II: a case study from the Sea of Marmara

Gaye Bayrakci · Carla Scalabrin · Stéphanie Dupré · Isabelle Leblond ·
Jean-Baptiste Tary · Nadine Lanteri · Jean-Marie Augustin · Laurent Berger ·
Estelle Cros · André Ogor · Christos Tsabaris · Marc Lescanne · Louis Géli

Received: 20 May 2013 / Accepted: 5 June 2014
© Springer Science+Business Media Dordrecht 2014

Abstract A rotating, acoustic gas bubble detector, BOB (Bubble OBServatory) module was deployed during two surveys, conducted in 2009 and 2011 respectively, to study the temporal variations of gas emissions from the Marmara seafloor, along the North Anatolian Fault zone. The echosounder mounted on the instrument insonifies an angular sector of 7° during a given duration (of about 1 h). Then it rotates to the next, near-by angular sector and so forth. When the full angular domain is insonified, the “pan and tilt system” rotates back to its initial position, in order to start a new cycle (of about 1 day). The acoustic data reveal that gas emission is not a steady process, with observed temporal variations ranging between a few minutes and 24 h (from one cycle to the other). Echo-integration and inversion performed on the acoustic data as described in

the companion paper of Leblond et al. (Mar Geophys Res, 2014), also indicate important variations in, respectively, the target strength and the volumetric flow rates of individual sources. However, the observed temporal variations may not be related to the properties of the gas source only, but reflect possible variations in sea-bottom currents, which could deviate the bubble train towards the neighboring sector. During the 2011 survey, a 4-component ocean bottom seismometer (OBS) was co-located at the seafloor, 59 m away from the BOB module. The acoustic data from our rotating, monitoring system support, but do not provide undisputable evidence to confirm, the hypothesis formulated by Tary et al. (2012), that the short-duration, non-seismic micro-events recorded by the OBS are likely produced by gas-related processes within the near seabed sediments. Hence, the use of a multibeam echosounder, or of several split beam echosounders should be preferred to rotating systems, for future experiments.

G. Bayrakci (✉) · C. Scalabrin · S. Dupré · I. Leblond ·
N. Lanteri · J.-M. Augustin · L. Berger · E. Cros · A. Ogor ·
L. Géli
Marine Geosciences, IFREMER, BP 70, 29280 Plouzané, France
e-mail: G.Bayrakci@soton.ac.uk

G. Bayrakci
National Oceanography Centre, University of Southampton,
European Way, Southampton SO14 3ZH, UK

I. Leblond
ENSTA Bretagne, 29806 Brest, France

J.-B. Tary
Department of Meteorology and Geophysics, University of
Vienna, Vienna, Austria

C. Tsabaris
Institute of Oceanography, Hellenic Centre for Marine Research,
Athens, Greece

M. Lescanne
TOTAL S.A., avenue Larribau, 64018 Pau Cedex, France

Keywords Acoustic monitoring · Gas emissions · Sea of Marmara · Water column acoustics · Nontectonic short-duration seismic signals · Ocean bottom seismometer

Introduction

Natural gas emissions from the seafloor is a common phenomenon that occurs worldwide, e.g. in coastal deposition features, delta fan deposits, hydrocarbon-bearing sedimentary basins and accretionary prisms (Judd and Hovland 2007). Over the last two decades, numerous studies have been carried out to recognize the importance of submarine gas emissions, in a large variety of submarine environments, e.g.: at the West Spitzbergen continental

margin (Knies et al. 2004; Mienert et al. 2005; Westbrook et al. 2008; Hustoft et al. 2009); at the Håkon Mosby Mud Volcano (Sauter et al. 2006; Foucher et al. 2010); at the Tommeliten and Gullfaks fields in the North Sea (Hovland and Sommerville 1985; Hovland 2007; Schneider Von Deimling et al. 2010, 2011); in the Santa Barbara Basin (Fischer 1978; Leifer and Clark 2002); in the Nile deep-sea fan (Dupré et al. 2008, 2010a; Bayon et al. 2013); in the Black Sea (Limonov et al. 1997; Greinert 2008); in the Marmara Sea (Kuscu et al. 2005; Géli et al. 2008; Gasperini et al. 2012).

The gases emitted from cold seeps are principally composed of methane. The importance of methane emissions for a number of societal (e. g. the assessment of the contribution of submarine methane sources in global budget) and environmental issues (e. g. hydrocarbon leak detection) conducting to economic ones, has fostered the interest of the scientific community for understanding the natural degassing processes from the seafloor. A variety of behaviors such as continuous, transient (periodic or sporadic) or eruptive, have been reported for seep activities, and temporal variations on scales ranging from tidal to sub-hourly periods have been documented (e. g. Leifer et al. 2004). The different causes proposed to explain the observed variations include: tides (Boles et al. 2001; Tryon et al. 2002); atmospheric (Mattson and Likens 1990) or swell-induced (Leifer and Boles 2005a, b) pressure changes; variations in bottom current conditions (Schneider Von Deimling et al. 2010); man made perturbations such as drilling operations (Wever et al. 2006); pressure changes in depth related to e.g. sediment instabilities; gas hydrates dissociation (Westbrook et al. 2009) and earthquake activity (Obzhirov et al. 2004; Mau et al. 2007; Kuscu et al. 2005; Kopf et al. 2010).

In parallel, experimental and theoretical, quantitative methods have been developed for the characterization of gas bubbles released from the seabed into the water column (e.g. Wheeler and Gardiner 1989; Sills et al. 1991; Briggs and Richardson 1996; Leighton and White 2011). In-situ methods for the quantification of the released gas include direct observations (e.g. Boles et al. 2001; Leifer and Boles 2005a, b); combination of gas flux-meters and pore-pressure measurements at the seabed interface (Kopf et al. 2009); measurements of dissolved gas concentrations in seawater samples from CTD equipment (which measure conductivity and temperature with depth) (Mau et al. 2007). Remote, water column acoustic studies are also carried out with the use of deep-towed side scan sonars (Merewether et al. 1985; Dupré et al. 2010a), ship-borne and deep-sea vehicle-mounted single-beam (Hornafius et al. 1999; Artemov et al. 2007; Foucher et al. 2010; Ostrovsky et al. 2008); with split-beam (Greinert et al. 2006) or multibeam echosounders (Schneider Von Deimling et al. 2007; Nikolovska et al. 2008; Schneider Von

Deimling and Papenberg, 2012, Dupré et al. 2010b); with horizontal-looking sonar mounted on a remotely operated vehicle (ROV) (Nikolovska et al. 2008); and with lander-based multibeam systems (Greinert 2008; Schneider Von Deimling et al. 2010).

Horizontally insonifying hydroacoustic devices enable the remote monitoring of the study area and do not affect the very sensitive fluid system and its environment (Greinert 2008). Advantages and drawbacks of multibeam versus splitbeam systems are discussed in a companion paper (Leblond et al. 2014). Multibeam and sonar systems mounted on ROVs cover a wider area and allow simultaneous monitoring of several emission sources. On the other hand, splitbeam systems have the advantage to be handled easily during deployment and recovery. They require less energy than multibeam systems, and offer thus longer recording periods. Their capacity to locate the target in three dimensions allows to calibrate them easily.

A splitbeam echosounder mounted on a pan and tilt system is used for the present study. We report observations from the Sea of Marmara seafloor and water column, obtained with an acoustic module demonstrator, hereafter referred to as BOB (Bubble OBServatory), specifically designed for the horizontal insonification of the water column. We discuss the spatial and temporal variations of seeps and explore the feasibility of assessing the volumetric bubble flows using this device. Then we propose to use the acoustic data to interpret non-seismic, transient signals recorded by an ocean bottom seismometer (OBS) located in the close vicinity of BOB.

Study area

The Sea of Marmara is an inland sea located in NW Turkey, linked to the Black Sea and to the Aegean Sea by the Bosphorus and the Dardanelle straits respectively. The Sea of Marmara consists in a narrow northern shelf, a broader southern shelf and a deeper middle part occupied by three deep basins called Tekirdag, Central and Cinarcik basins, separated by two highs, respectively the Western and the Central highs (Fig. 1) (Rangin et al. 2001). The Sea of Marmara is considered to be a seismic gap, between two strike slip segments of the North-Anatolian Fault (e.g. Sengör et al. 2005), which ruptured during the Ganos (1912) to the west and Izmit and Duzce (1999) earthquakes to the east (Le Pichon et al. 2001).

After the 1999 destructive earthquakes, the Marmara Sea has been extensively surveyed with numerous marine expeditions conducted. In the Gulf of Izmit repeated surveys showed that the intensity of methane emissions increased after August 17th, 1999, Mw 7.4 earthquake (Alpar 1999; Kusçu et al. 2002; Kuscu et al. 2005). The

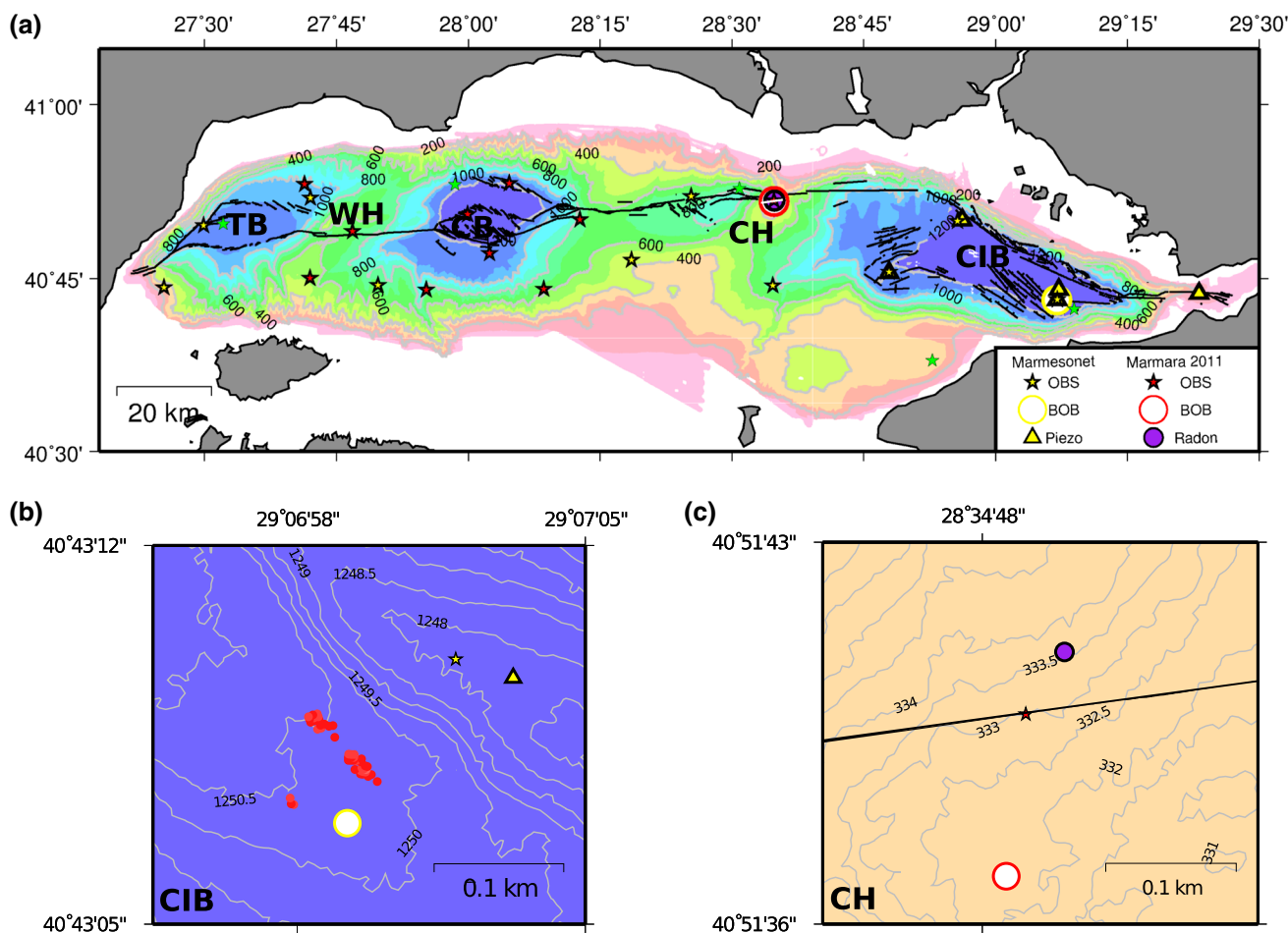


Fig. 1 a Bathymetric map (Rangin et al. 2001) of the Marmara Sea with 200 m contours. Instrument deployment sites for the Marmesonet 2009 and Marmara 2011 expeditions are indicated. Submarine faults scarps after Grall et al. (2012) are represented in black. TB Tekirdag Basin, WH Western High, CB Central Basin, CH Central

High, CIB Cinarcik Basin. Zooms on the areas of b Marmesonet 2009 deployments. Gas bubble sources (in red) observed over three cycles, from the BOB Marmesonet 2009 data, superimposed to the seafloor bathymetry c Marmara 2011 BOB module deployments. Black line indicates the location of chirp profile shown in Fig. 13

widespread occurrence of free gas within the shallow sediment layers and the water column was documented with deep-towed side scan and towed singlebeam sonars (Géli et al. 2008), sub-bottom profiler data (Tary 2011, pp 199–218) and ship-borne multibeam echosounder data (Dupré et al. 2010b). Cold seeps and associated seabed expressions such as methane-derived carbonates (Crémière et al. 2013), dark reduced sediment patches (resulting from the anaerobic oxidation of methane, Boetius et al. 2000) and bacterial mats, were discovered in relation with the fault zone (Armijo et al. 2005; Zitter et al. 2008) which, confirmed the link between faults and fluid venting (Géli et al. 2008). The emitted gas at the Marmara seafloor is mainly composed of methane with the presence of gas hydrates at the Western High (Bourry et al. 2009).

In the Marmara Sea, sea-level variations are mainly due to meteorological and oceanographic conditions of the region. The entire sea is not large enough to generate its

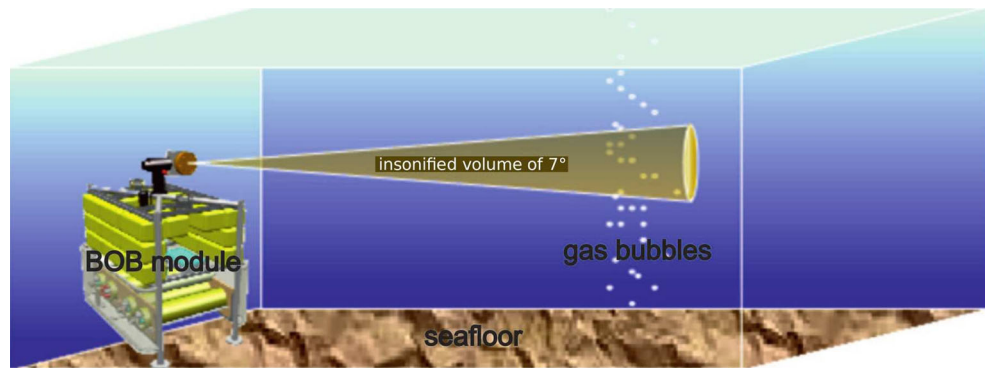
own tides. The co-oscillations with the neighboring seas are limited due to the presence of two shallow, narrow and long straights and a two-layered water exchange system. Hence, tide amplitudes do not exceed 3 cm in the Marmara Sea (Yüce 1993; Alpar and Yuce 1997).

Bubble observation (BOB) module: instrument description and methods

Instrument description

The bubble observatory (BOB) module is a standalone acoustic module developed by IFREMER and equipped with a Simrad ER 60 echosounder and a 120 kHz split-beam transducer for upward or horizontal insonification of the surrounding water column at the seafloor. The deployment depth range is constrained by the pressure

Fig. 2 Schematic description of the Bubble Observatory (BOB) module. The tilt angle is set to 4° upward in order to avoid seafloor reflections. The pan angle is set to 7°



qualification of the transducer and limited to 1500 m below sea-surface. BOB could be connected to a cable seafloor observatory considering an average power consumption of 30 W (24 V) and an average bandwidth of 36 Kbits/s if real-time data processing were required. However, BOB was designed to be used as a demonstrator to provide a preliminary acoustic exploration of a site of interest and to test the feasibility of detection of different targets. Therefore, it could be used to carry out a cost-benefit analysis of acoustic data monitoring before the installation of a cable seafloor observatory. As a demonstrator, BOB can be easily deployed with a vessel A-frame and provides autonomous and continuous data acquisition for at least 3 weeks. The echosounder transducer is mounted on a “pan and tilt system” allowing BOB to steadily insonify a fixed direction or to scan different directions.

Data presented here were acquired by using a horizontal scanning option according to the following parameters and strategy: data acquisition during a given duration T from one horizontal angular sector of 7° by “pinging” every 1.5 s with a pulse duration of 1024 μs ; 7° clockwise rotation to insonify the next, near-by angular sector of 7° and so forth. When the full angular domain is covered, the “pan and tilt system” rotates back to its initial position, in order to start a new cycle (Fig. 2). The tilt was set equal to 4° upward in order to avoid reflections from the seafloor such as small-scale relief.

Echograms

The acoustic data recorded by BOB are displayed as “echograms” (see example in Fig. 3), which characterize the back-scattered signals from one given angular sector of 7° recorded during a given record duration of “ T ” (see section 4, T is 72 and 60 min for the Marmesonet 2009 and the Marmara 2011 surveys, respectively). Echograms (e.g. Fig. 3) represent the volume back-scattering strength (S_v), the logarithmic expression (in dB) of the volume back-scattering coefficient (s_v) which is a summation of the contribution from all targets within the sampling volume

(see Leblond et al. 2014). The x-axis on echograms represents time, which is obtained by multiplying the ping number by 1.5 s, the time interval between pings. The y-axis represents the horizontal distance from the BOB module. The distance is obtained by multiplying the number of samples by 0.194 cm, the distance travelled by the echo between two successive time samples.

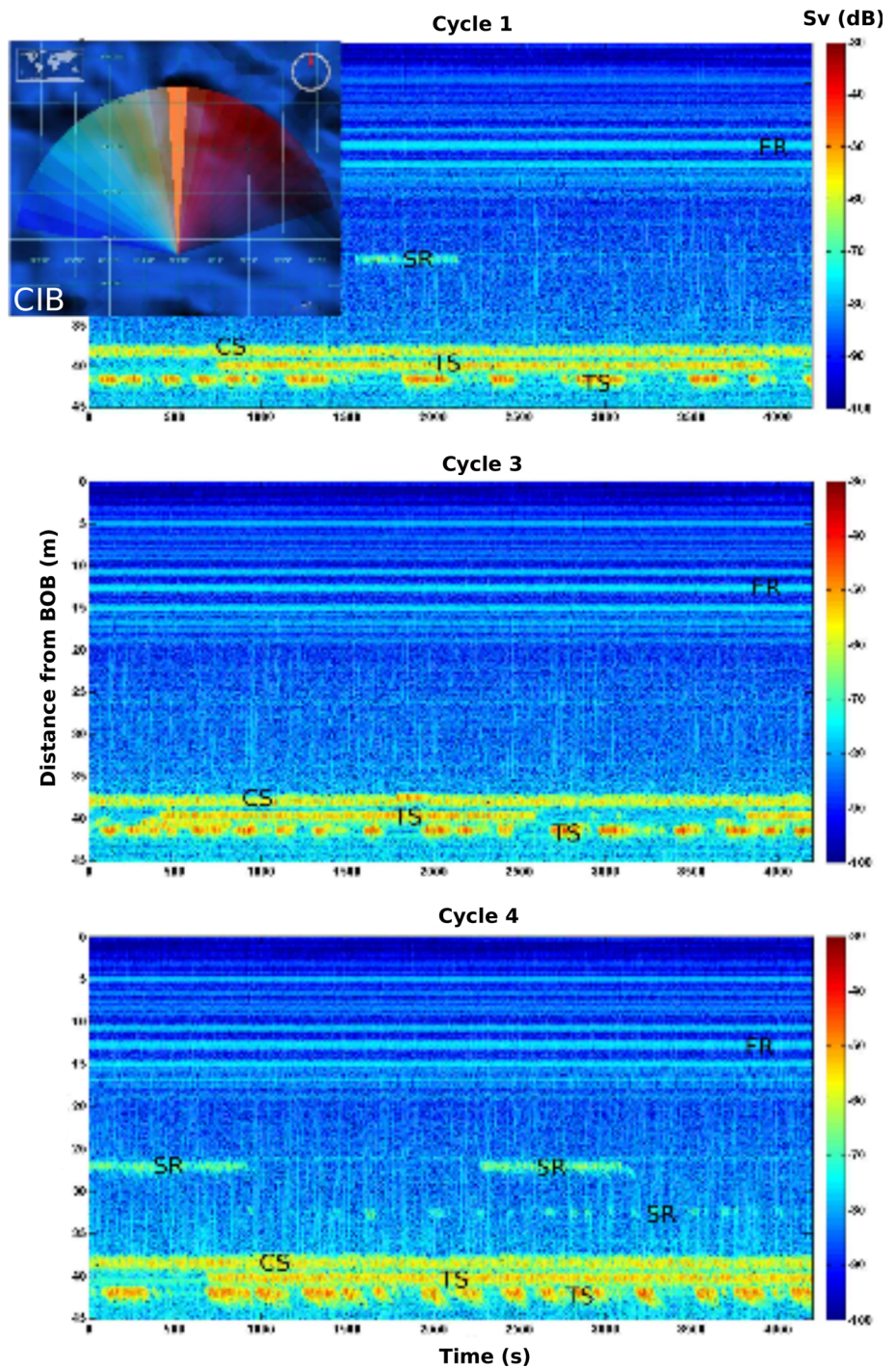
Echo-integration

Echoes may either come from single gas bubbles, well enough separated from their neighbors, either from clusters of bubbles and possibly coming from different sources. Therefore, the bubble abundance within the insonified area cannot be approached by simply counting the individual bubble echoes. The alternative technique is the echo-integration (Dragesund and Olsen 1965). This technique allows the quantification of the target (e.g. gas bubbles or fish bladders) density in the acoustic beam, whether or not the received signal contains overlapping echoes from different sources.

The echo-integration was performed on separate files per sector, with the water column acoustics code Movies 3D (IFREMER[®]). No filtering has been applied to echograms since the gas bubble sources were easily recognizable on the raw data. For each given sector, the echo-integration was carried out on layers of 2 meters in the horizontal range and with ESU (Elementary Sampling Unit) equal to the whole record period of one sector (i.e. 72 min and 60 min in 2009—Fig. 4 and in 2011—Fig. 5 respectively). The echo-integration per layer allows locating the backscatters in horizontal distance within the insonified sector of 7° . The maximum display distance, above which no signal can be extracted from the background noise, was 80 m and 110 m for the Marmesonet 2009 and the Marmara 2011 data, respectively.

The result of echo-integration is expressed in Mean Volume Back-scattering Strength (MVBS) (Simmonds and MacLennan 2005), hereafter noted S_v which is the logarithmic measure of the mean of the volume backscattering

Fig. 3 Example of acoustic data acquired by the BOB module (Marmesonet expedition 2009). Echograms of the 1° N oriented sector are shown over three cycles (1, 3 and 4). *FR* Fix Reflector, *SR* reflector imaged by secondary lobes, *CS* continuous source, *TS* transient source



coefficient s_v [$S_v = 10 \times \log_{10}(\text{mean}(s_v))$], whose units are dB re 1/m. In the following Figs. 4 and 5, echo-integration results are expressed in MVBS. Since a linear relationship between bubble density and echo-integrated intensity is expected (Foote 1983), the observed MVBS variations can be seen a proxy for the flux rate variations.

It is important to note here that during the two field expeditions described hereafter (i.e. Marmesonet 2009 and Marmara 2011) the echosounder was calibrated at

atmospheric pressure with the procedure described by Foote (1982) and Foote et al. (1987). No in situ calibration was performed. However, before in situ deployments, many tests considering various bubble sizes (including the ones observed at the Cinarcik Basin and the Central High) were carried out at \sim atmospheric pressure during pool experiments. The impedance contrast between the gas bubbles and the water is high enough that influence of pressure is negligible. Hence, the differences between the

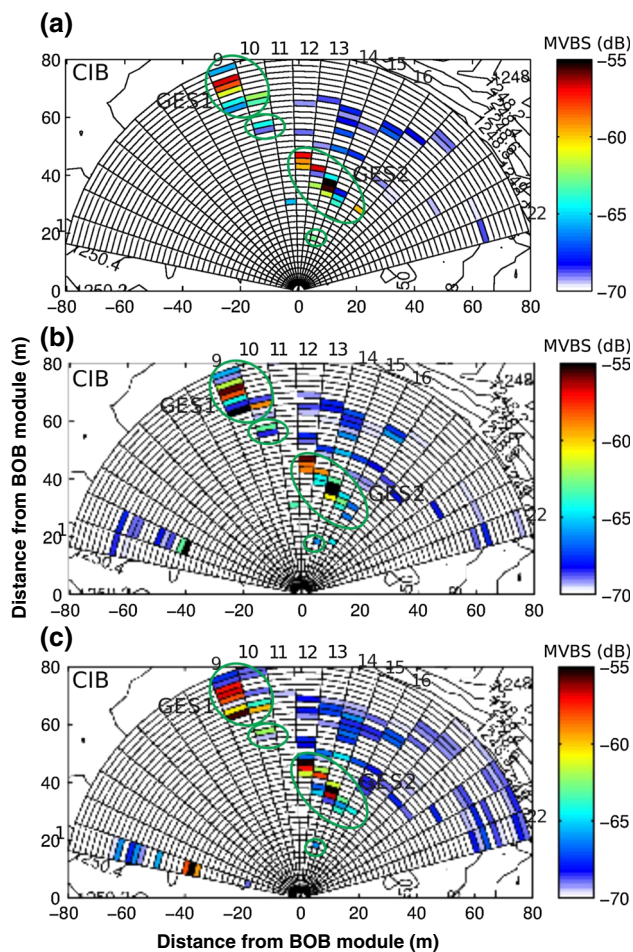


Fig. 4 Echo-integration results of Marmesonet 2009 BOB data in the Cinarcik Basin. The threshold applied for the echo-integration is -70 dB. **a** Cycle 1, **b** Cycle 3 and **c** Cycle 4. Persistent gas emission sites (GES) are shown in solid green circles

backscattering of bubbles of same sizes but at different pressures can be disregarded (Greinert and Nutzel 2004).

Computation of flow rates

For each identified gas bubble source, flow rates were computed using the specific methodology developed in the companion paper of Leblond et al. (2014) and based on inverse modeling, as used in fishery acoustics. Volumetric flows presented in the present paper are derived from an average of the results obtained using the different models tested in Leblond et al. (2014): Stanton model for gaseous prolate spheroid with equivalent sphere, Stanton model for gaseous sphere with equivalent sphere, Stanton model for gaseous sphere with multiplicative factor Stanton (1989) and Medwin model for gaseous sphere with multiplicative factor (Medwin and Clay 1998; see also Leblond et al. 2014). The physical parameters required for the inverse

modeling, the size distribution of gas bubbles and the ascent rate, were estimated as hereafter described.

Tentative in-situ estimation of bubble sizes

In-situ visual estimations of the bubble size were obtained using the video camera records that were collected in 2007 with the Nautilie submersible (Henry et al. 2007). During four dives (respectively in the Tekirdag Basin, in the Cinarcik Basin, on the Western High and on the Central High, Table 1), gas bubbles were sampled using the specifically designed, PEGAZ gas sampler (Bourry et al. 2009), which allows in situ fluid sampling with conservation of the initial pressure. PEGAZ consists in a glass cone, for trapping the bubbles over the gas source. When the cone is full, the gas is stored in a titan container, the opening of which can be remotely triggered from the submersible. The PEGAZ glass cone is clearly visible on the video records, allowing a 8 mm mark on the glass to be used as a reference scale for measuring the bubble sizes with the ImageJ software (Fig. 6). In order to allow a statistical estimation, the bubble size measurements have been systematically repeated, every time when the camera moved to another plan. Limitations were due to: (1) the image resolution which, for smaller bubbles, didn't allow zooming; (2) the image blurring; (3) water turbidity and the presence of suspended particles; (4) the combined effect of camera's obturation speed and the bubbles ascent speed; and (5) the difficulty in the identification of isolated bubbles and in not considering them twice in consecutive video images. A great number of measurements were performed. The resulting histogram shows a relatively well-defined Gaussian distribution of measurements, allowing an average value to be computed. In the Cinarcik Basin (1,248 m of water depth), up to 100 observations of isolated bubbles yield an average bubble diameter of 5 mm (within an interval of 1–8 mm, Fig. 6c). On top of the Central High (347 m water depth), only 13 measurements were made, due to the intense water turbidity, yielding a bubble diameter of 3.7 mm (varying between 1 and 6 mm, Fig. 6d). Although these measurements were made on videos recorded in 2007, we consider that they provide an acceptable estimate for average the size of the visible bubbles that were present in the Cinarcik Basin in 2009 and on top of the Central High in 2011. It is important to note here that we do not take into account the possible effect of non-visible, micro-bubbles (of radius <0.1 mm) that could induce resonance phenomena at 120 kHz.

Tentative estimation of the ascent speed of bubbles

The sensitivity of flux calculations to ascent rate is discussed in a companion paper (Leblond et al. 2014). The ascent rate of gas bubbles is closely related to bubble size

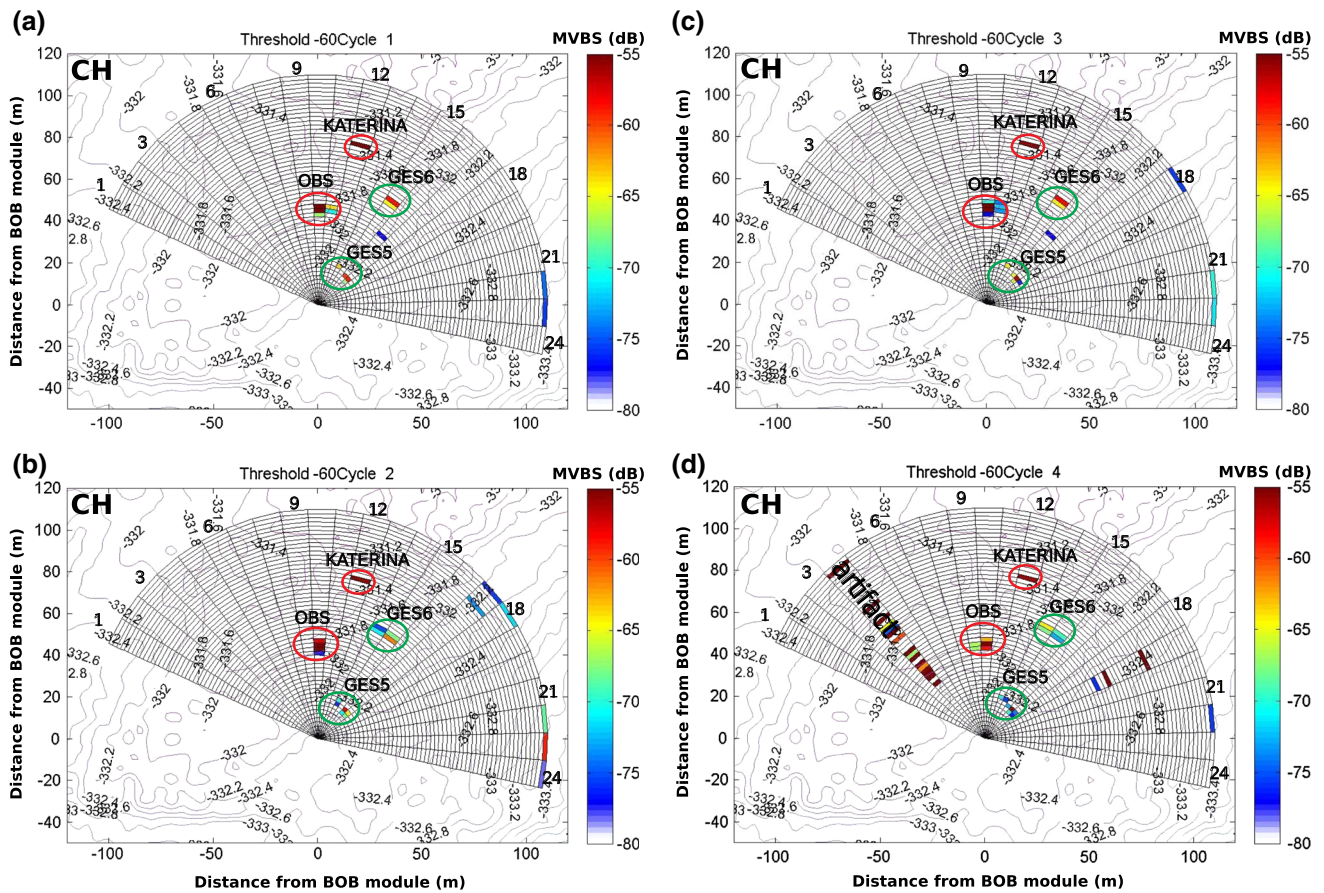


Fig. 5 Echo-integration results of Marmara 2011 BOB data over the Central High. The first four cycles are shown as polar diagrams over the seafloor bathymetry. Threshold applied for the echo-integration is

−60 dB **a** Cycle 1, **b** Cycle 2, **c** Cycle 3 and **d** Cycle 4. Natural gas sources are surrounded in *green*. Echoes from OBS 04 and KATERINA (the radonmeter) are surrounded in *red*

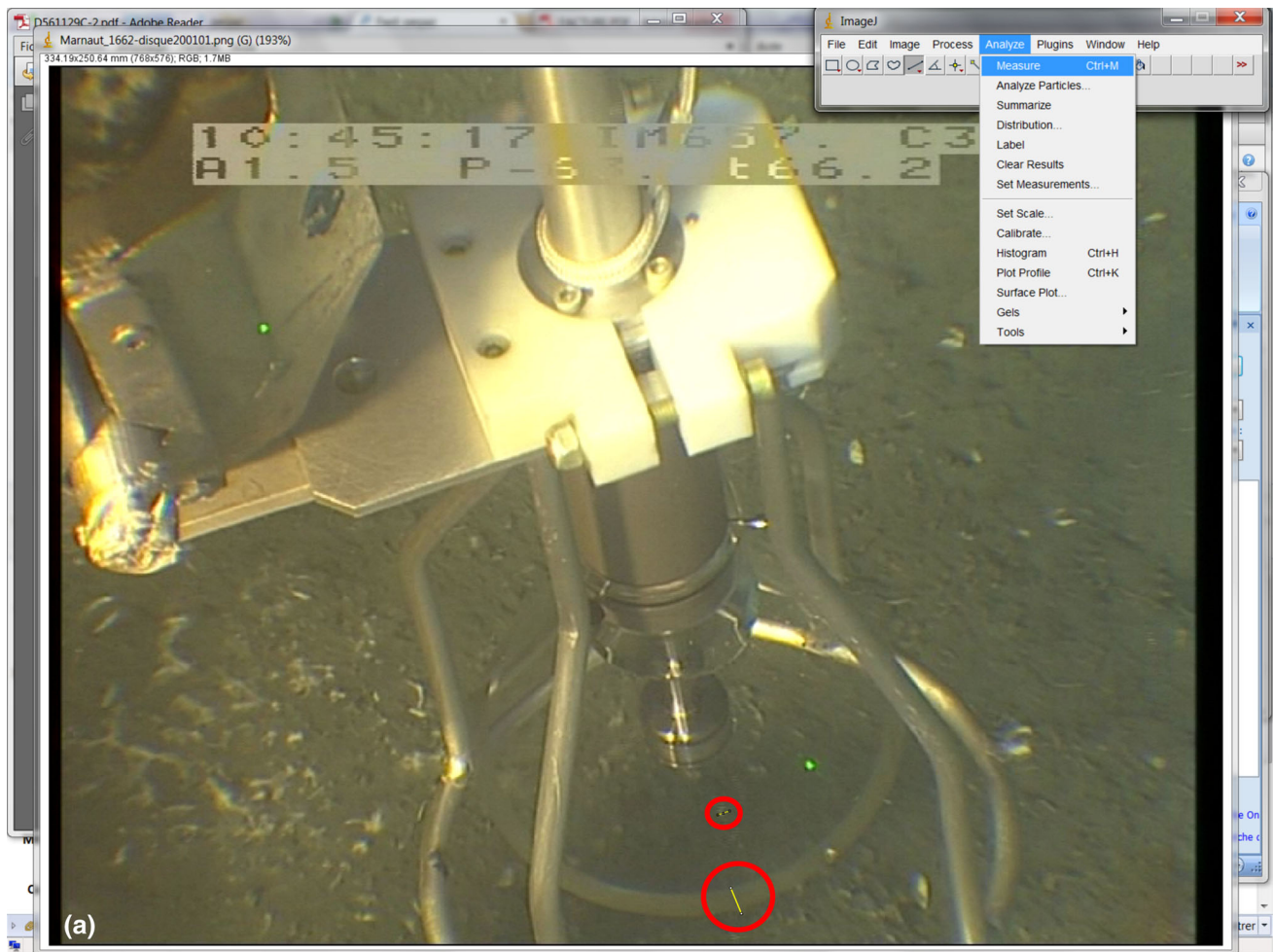
Table 1 Measurements of individual bubble size derived from videos recorded with submersible Nautilie during the Marnaut cruise of R/V L’Atalante (2007)

Dive number	Number of measurements on individual bubbles	Water depth (m)	Area	Latitude	Longitude
1647	91	1,145	Tekirdag Basin	N40°44.43'	E027°21.32'
1659	100	1,248	Cinarcik Basin	N40°38.01'	E029°00.61'
1662	100	657	Western High	N40°44.38'	E027°35.53'
1664	13	347	Central High	N40°43.94'	E028°25.27'

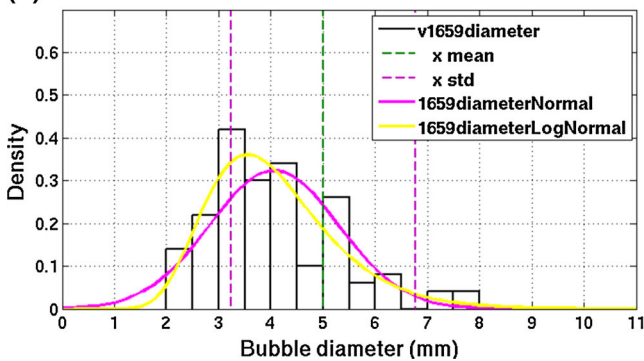
and to the environmental variables such as sediment particles, organic matter and oil (Clift et al. 1978; Greinert et al. 2006). Based on theoretical calculations (Clift et al. 1978), ascent rate values may be inferred from the average bubble diameter that was measured in situ e.g. 5 and 3.7 mm in Cinarcik Basin and Central High respectively; imply an ascent rate of 17–18 cm/s.

The ascent rate was also tentatively estimated using the track of echoes displayed on an echogram collected with a vertically insonifying echosounder as described e. g. by Greinert et al. (2006). During the Marmesonet 2009

expedition, sediment cores were taken where the BOB was deployed in 2011. Gas bubbles were expelled in the water column, as the core was pulled out from the surface sediments. The ascent rate that was inferred from the echoes of the rising bubbles in response to the vertical 12 kHz shipboard echosounder was ~20 cm/s (Fig. VIII.3 in Géli et al. 2009). This value is consistent with in situ visual observations of bubbles escaping (17–18 cm/s) after penetration in the sediments of 50 cm long cores by the Nautilie submersible. Bubble size and shape from induced escapes may be different from natural emissions, as



(b) Nautilie Marnaut dive 1659 (depth: 1248 m) Cinarcik Basin



(c) Nautilie Marnaut dive 1664 (depth: 347 m) Central High

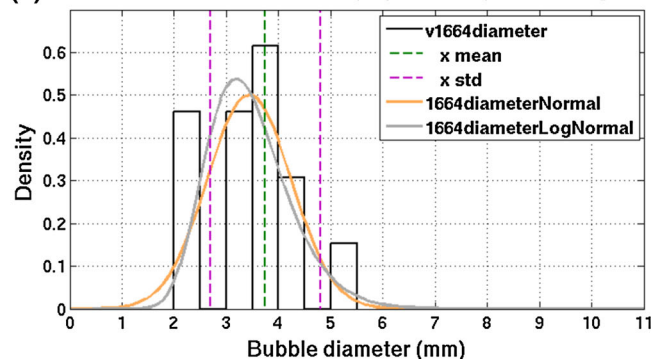


Fig. 6 Gaz sampling using the PEGAZ system with Nautilie submersible in the Central High during Marnaut cruise of R/V L'Atlante (Henry et al. 2007). **a** Image from a video taken by Nautilie

submersible, showing the 8 mm reference frame of the PEGAZ tool. **b** Bubble size distribution at the Cinarcik Basin. **c** Bubble size distribution at the Central High

environmental conditions, e.g. upwelling, may impact the bubble ascent. Besides these differences, the orders of magnitude are comparable (e. g. 18 vs. 20 cm/s) and consistent with other estimates proposed by various authors in different environments. Therefore, a value of 18 cm/s is used here for flux calculations.

Results and discussions

Marmesonet 2009 dataset

During the Marmesonet cruise, in 2009, 22 angular sectors of 7° each, were successivelyinsonified during 72 min

each. As a result, an angular domain of 154° (divided in 22 sectors of 7°) between 285° N and 70° N, was insonified during every single cycle of 26 h. At the end of each cycle the transducer turned to the first sector in order to begin to acquire a new cycle. Four weeks of data acquisition were initially scheduled, unfortunately only four daily cycles were recorded, due to a technical failure. Results from the second cycle of Marmesonet dataset were not considered in this paper since anomalously high backscattering values were found that are not yet fully understood.

In order to map the distribution of seafloor gas emissions at the scale of the Sea of Marmara, ship-borne multibeam survey of the water column was also conducted during the Marmesonet 2009 expedition (Dupré et al. 2010b). Seafloor and water column data were acquired with the Simrad EM302 multibeam echosounder (27–33 kHz, 288 beams, beam width of $1^\circ \times 2^\circ$ and a pulse length of 2 or 5 ms) with automatic swath width control and equidistant sounding pattern over water depths varying from 300 to 1270 m. Water column amplitude values were stored along more than 4,500 km acoustic tracks. Approximately 70 % ($\sim 2,900$ km²) of the North Marmara Trough (northern and deeper part of the Marmara Sea where the seafloor depth is >300 m) has been covered in 21 days of acquisition (Dupré et al. 2010b). Sub-bottom profiler (1.8–5.3 kHz) data covering the whole North Marmara Trough was also acquired during the Marmesonet 2009 expedition.

An ocean bottom seismometer (OBS 09) was deployed 150 m away from the BOB module (Fig. 1a, b). Unfortunately, the data are affected by a characteristic noise due to heavy ship traffic preventing from studying correlations between the acoustic and the seismologic data.

On the three echograms displayed in Fig. 3, fixed reflectors (FR) such as bathymetric features appear with low values of -75 dB within a distance of less than 20 m from the transducer. These reflections are imaged by secondary lobes and hence appear with lower S_v values than the other scatters. These can be easily distinguished from the other targets such as gas bubble sources, thanks to their static and continuous appearance during the whole record period of the sector. In contrast, gas bubble sources appear as pixels exhibiting variations in S_v (between -40 and -65 dB), likely due to variations in gas flow rate and in the number of insonified bubbles. On the echograms, gas-related reflectors can be seen at a distance of, respectively, 39, 41 and 43 m from the transducer with S_v values varying between -40 and -65 dB. These three gas bubble sources have different behaviors. The gas source located at 39 m from the BOB module appears continuous over the 72 min record period and over four cycles (with more than 1 day interval between cycles). The second source located at 41 m from BOB is active over about 55 min (during the first cycle). It is not observed at the beginning and at the

end of the first cycle, suggesting that it is a transient source. The emission duration varies among the cycles from ~ 55 min (cycle 1) to ~ 38 min (1,500 pings, cycle 3) and more than 1 h (cycle 4). The third and farther source is also a transient but with a shorter duration of gas emissions, varying between 2 and 15 min approximately. The acoustic data acquired by BOB in the Cinarcik Basin during the Marmesonet 2009 survey show therefore that the gas emission may be continuous or transient with a variety of emission durations. The echoes from gas bubbles cannot be confused with that from benthos or fish bladders, as it is unlucky that fishes stay immobile during one hour in the water column. The similarity of the echogram patterns and the backscatter values observed in situ and during pool experiments (Leblond et al. 2014) brings an evidence that the observed echoes are related to gas bubbles escaping from the seabed.

The main source of misinterpretation of echograms may thus be the echoes from the gas bubbles within the neighboring sectors imaged with the side-lobes (see SR label in Fig. 3). The sector-rotated configuration allowing the insonification of a larger area increases on the other hand the probability of such misinterpretation. But with a careful joint-analysis of echograms of neighboring sectors, it is still possible to identify the real places of reflectors with the amplitude difference between echoes imaged by the main and side-lobes.

The echo-integration results of Marmesonet 2009 data (Fig. 4) show four distinct persistent and three transient Gas Emission Sites (GES). GES1 located on the 9th and 10th sectors is observed on several layers between 64 and 80 m distance from BOB suggesting a site with multiple sources. GES2 spreads over several sectors (sector 12, 13, 14, 15 and 16) between 30 and 50 m distance from BOB and probably originates from several gas sources. Sources within GES2 appear well aligned along a NW–SE orientation.

GES3 and GES4 seem to be associated with a single source or several small sources spatially concentrated. They are respectively located within sector 10, at a distance of 56–58 m from BOB, and within sector 14, at a distance of 16 m from BOB. These sources have smaller MVBS values than GES1 and GES2, because their emission type is not continuous but transient. Since the echo-integration is carried out on an elementary sampling unit (ESU) of 72 min, they appear with lower MVBS values. The other layers, where some MVBS values range between -70 and -65 dB, correspond to other gas related sources with transient emission type or to some reflections from fixed reflectors such as small-scale bathymetric highs imaged by side lobes.

All above described GESs exhibit spatial and temporal variations over the 4 days-long record period. A hypothesis could be that the sources forming one given GES could be

linked at depth, and split into several fractures in the upper sedimentary layers, as shown in the literature (e.g. Boles et al. 2001; Tryon et al. 2002; Leifer et al. 2004; Leifer and Boles 2005a, b Schneider Von Deimling et al. 2010).

Tidal control on gas emission as a result of changing hydrostatic pressure has been shown by Boles et al. (2001) and Schneider von Deimling et al. (2010) in shallow water depth (of 67 and 70 m respectively). The present data set acquired with an interval of 25 h between two consecutive insonifications of the same sector does not allow us to check the tidally driven flow oscillations. However, in the Sea of Marmara, tide amplitudes do not exceed 3 cm (Yüce 1993; Alpar and Yuce 1997) and the hydrostatic pressure variations induced by sea-level variations of 0.002 % of the total depth are not significant.

The gas bubble sources detected during the Marmesonet 2009 expedition are aligned along a Northwest orientation (Fig. 1), which is coherent with the orientation of the bathymetric features, as well as with the orientations of the sea-bottom traces of the antithetic normal faults observed at the southern part of the Cinarcik Basin (Laigle et al. 2008). This suggests that the gas emission pattern follows a high permeability zone controlled by the main structural trends.

Marmara 2011 dataset

During the Marmara 2011 expedition, a seafloor observatory, comprising a BOB module and an OBS from IFR-EMER, and one radonmeter named KATERINA from HCMR (Greece), was deployed with the R/V Yunus over the north-eastern part of Central High near 40°N 51.6855', 28° E 34.8339' at a depth of ~330 m (Fig. 1c). The OBS 04 was placed approximately 59 m away from the BOB module while the KATERINA radonmeter was placed approximately 38 m away from OBS 04. Instrument positions may have some uncertainties (<20 m), since R/V Yunus is not equipped with a dynamic positioning system. The acoustic echoes from the KATERINA structure were very useful to precisely locate the other instruments and acoustic events recorded by BOB. The OBS provided 3.5 month of data recording, from April 15th to July 31th 2011. Nine additional OBSs, covering the western half of the Marmara Sea were deployed and acquired seismologic time series of 3.5 months as well.

Bubble Observatory was programmed to acquire one month of acoustic water column data, from April 12th to May 12th, 2011. The log data shows that the EK 60 split-beam echosounder as well as the pan and tilt system on which the transducer was placed did work correctly during one month. However, due to a problem on data storage device, only 7 days of data between 12th and 19th of April 2011 could be extracted. The echosounder (beam

width = 7°, pulse length ~1 ms, interval between two successive pings = 1.5 s) and the pan and tilt (7° and 4° upward, respectively) configuration was the same as for the Marmesonet 2009 survey. The record period of one 7° sector was 1 h and 24 angular sectors of 7° covered the geographic angular sector between 291° N and 99° N during one cycle of 24 h. A total of 7 cycles was therefore collected in 7 days.

Figure 5 shows the echo-integration results of the Marmara 2011 acoustic data over the first 4 cycles. On each cycle, OBS-04 appears on the 10th sector of the polar diagram, 46 m away from BOB module, and the radonmeter on the 12th sector, 78 m away from BOB. Both instruments appear with high MVBS (−55 dB) compared to other echoes corresponding to gas bubble sources (−80 to −57 dB). Two continuous and one transient gas emission sources were identified over the whole record period (Fig. 5): GES5 spreads between the 13th and 18th sectors, 16–22 m distance from the BOB module. It seems to be composed of two separate small sources. No echo was observed on the 15th sector at 16–22 m distance from BOB during first three cycles, suggesting that the bubble streams are sufficiently apart from each other not to be detected by the 7° acoustic beam gap. On the contrary, during cycle 4, two sources appear linked. This could be the effect of sea-bottom currents. During the first three cycles, the western small source appears only on sector 14 and the eastern one appears on sectors 16–17 (and 18 on the 3th cycle). It is only during cycle 4, that the western source spreads on the 13th sector, and that the eastern one spreads on the 15th sector suggesting a westward bubble dispersion that could be caused by sea-bottom current having a westward component during the record periods of these sectors.

No three dimensional current meter data are available to check this hypothesis. The currents would change the three-dimensional shape of a flare by adding a horizontal component to the almost straight upward migration of bubbles, which would result in tilted or bent flares (Greenert et al. 2006). In the literature, an average sea-bottom current speed of 25 cm/s is reported for the Marmara Sea (Ergin et al. 1991), which is enough to deviate the bubble train by an angle of more than 45°, assuming an ascent speed of 20 cm/s.

GES6 is observed on the 15th sector, at a distance of 60 to 62 m from BOB during cycles 1 and 3 whereas during cycles two and four it is observed on both 14th and 15th sectors. When the source is observed only on sector 15, higher MVBS values are measured within the 62 m layer (−58.7 and −58.5 dB respectively during cycles one and three). This is not the case during cycle two and four where the highest value corresponds to sector 15 within the 60 m layer and to sector 14 within the 62 m layer respectively. The observed variations at GES6 are coherent with those

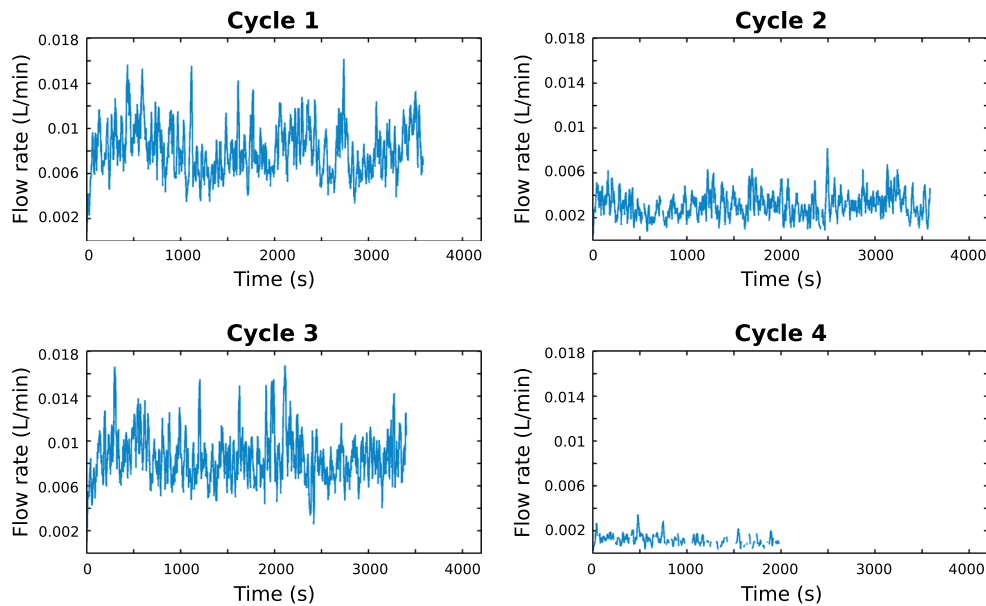


Fig. 7 Flow rates computed with the methodology described by Leblond et al. (2014) for the GES6 over four cycles. Notice that for cycles 2 and 4, the calculated flow rates are significantly lower than the ones for the cycles 1 and 3

observed at GES5, which suggests that such variations could be caused by sea-bottom currents rather than by temporal variations of the gas emission. This suggestion also holds when considering flow rates at GES6 (Fig. 7). Higher flow rates are retrieved for cycles 1 and 3 where the source is observed in one sector. The currents may affect the flux calculations not only because the whole extend of the source may not be imaged simultaneously but also because of the bubbles that may migrate out of the acoustic main-lobe. In this case, the computed flow rates, between 2 and 16 ml/min, are likely to have been underestimated. Notice that the flow rates shown in Fig. 7 are not corrected to atmospheric pressure. Before any comparison with other methane emission sites at different depths and temperatures, the compressibility of methane gas needs to be considered (e. g. Duan et al. 1992a, b) and the comparison has to be done at a certain reference pressure (e.g. sea surface) (Greinert and Nutz 2004) and temperature.

Changes in bottom currents speed may also affect the bubble size. Enhanced currents support the detaching of bubbles from the sediment grain resistance creating smaller bubbles. The presence of micro-bubbles would rule out the relationship between S_v and the gas flux (Schneider Von Deimling et al. 2010). At a depth of 1,000 m, a bubble with a radius of 0.27 mm will be resonant with 120 kHz echosounder (J. Greinert, Geomar, Germany, personal communication, 2014). Micro-bubbles with <0.5 mm radius are too small to detach from the seafloor because their buoyancy is too small to overcome the resistance of the sediment grains (Schneider Von Deimling et al. 2010). However, micro-bubbles may also form when large

bubbles break up in the water column and rise with a smaller velocity, therefore entering in the beam gradually, whereas larger bubbles would induce a sudden increase of S_v on the echograms (Schneider Von Deimling et al. 2010).

On the echo-integration results, unlike the radonmeter, the OBS appears on several sectors and several layers (Fig. 5). This could be due to the position of the OBS. If the OBS were not entirely located within a layer along a sector but located between two sectors and/or between two layers, its echo would appear on two layers and/or on two sectors. This could also be due to secondary lobes, which might image backscatters from neighboring sectors. However, in these two cases, no significant spatial and temporal variations would be observed in the echo of the OBS. In the present case, the high MVBS part of the echo of the OBS always appears 46 m away from the OBS, on the 10th sector. But, during cycles 1 and 3, the rest of the echo appears on the 11th sector whereas, during cycle 4, it appears on the 9th sector. During cycle 2, the echo appears only on the 10th sector but instead of being on three layers, it appears on four layers.

On the echograms (Fig. 8), the echo from the radonmeter appears flat and non-pixelated, with an S_v of -50 dB for all cycles. This shows that changing currents do not imply significant variation in the amount of suspended matter, which might affect the scattering of high frequency sources (Schneider Von Deimling et al. 2010). The echo from the OBS appears with (1) a flat looking part between 43 and 47 m distance from BOB with a high S_v value (-50 dB) on every cycles and (2) a pixelated part, which is similar to the echoes of gas bubble sources. The pixelated

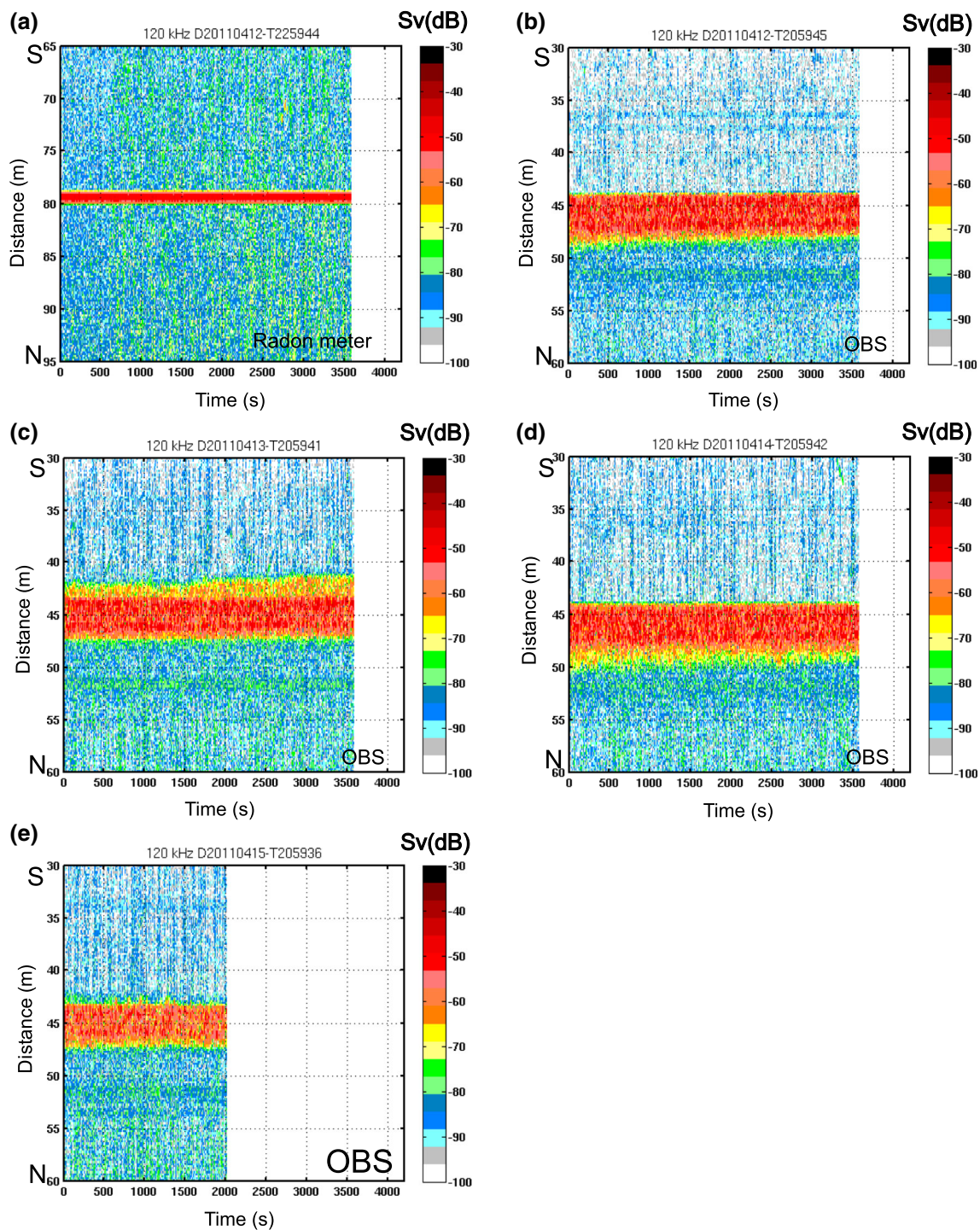


Fig. 8 **a** Zoom on the echo of the radonmeter, during cycle 1. **b–e** Zooms on the echo of OBS 04 during cycles 1–4, respectively

part of the OBS echo displays spatial and temporal variations. During cycles 1 and 3 it appears to the north of the main echo, whereas during cycle 2, it appears to its south. On cycle 4, the main echo appears pixelated over a smaller distance compared to the other cycles. These observations suggest the presence of a gas source below OBS 04.

Comparison between near-bottom and ship-borne water column acoustic data

The water column above the Marmara Sea was investigated in 2009 during the Marmesonet survey using the EM302 Kongsberg multibeam echosounder of R/V Le Suroit

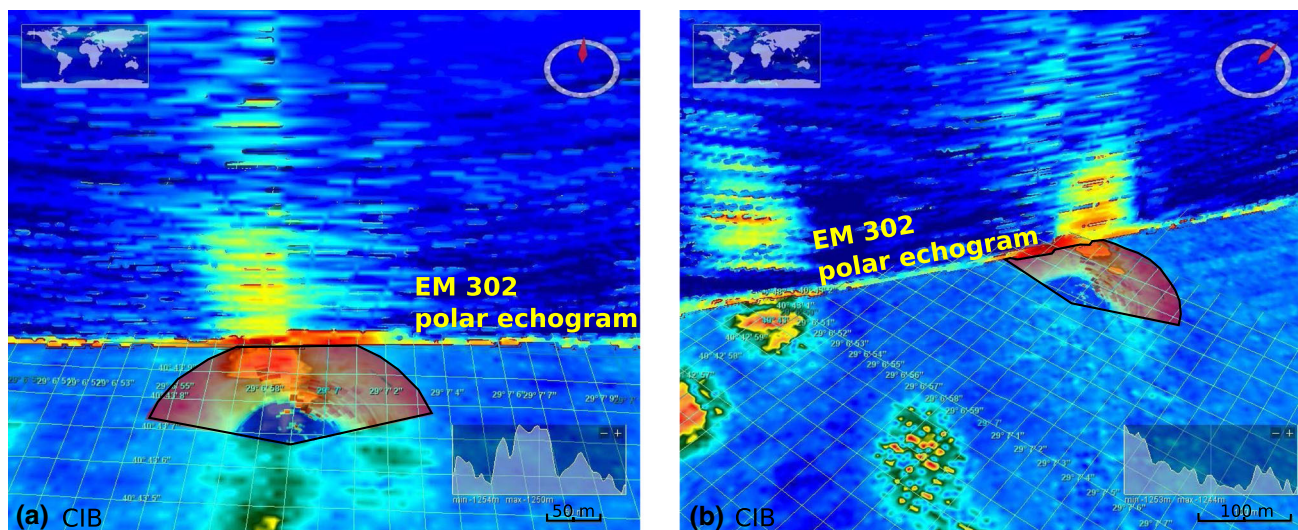


Fig. 9 Mosaic view of the echo-integration results in the Cinarcik Basin based on the EM302 multibeam data collected with R/V Le Suroit in 2009, superimposed with the Marmesonet 2009 BOB echo-

integration results. A polar echogram inferred from the EM-302 multibeam data is also shown in the *water column*. **a** along a N–S profile, **b** a NW–SE profile

(27–33 kHz) (Dupré et al. 2010b). At the Cinarcik Basin, the location of flares shows NW–SE oriented gas emissions, simultaneously identified by the ship-borne multibeam EM302 echosounder and by BOB (Fig. 9). Echoes recorded up to 80 m from the BOB module delineate the southern border of the gas emission site identified in EM302 data. For distances greater than 80 m, scattering layers were not taken into account due to a weak signal to noise ratio. On every EM302 passes with different azimuths above the BOB module, gas emission sites retrieved by BOB were also retrieved by the EM302. The gas flares are visible on the polar echograms acquired with the EM302 multibeam echosounder (Fig. 9).

In 2011, BOB recorded echoes from numerous gas bubble sources from the Central High, that were previously identified on 2009 ship-borne multibeam data, suggesting that some of the gas emissions are continuous at the year scale (Fig. 10, see also Dupré et al. 2010b). The site where OBS 04 was deployed in 2011 was also identified as a gas emission zone in 2009, supporting the hypothesis that OBS 04 was actually sitting on a natural gas source. In 2009, this source appeared to be continuous over tens of meters, based on EM302 data. In 2011, on the BOB results, the source appears to be punctual and located above the OBS. The difference between EM302 (2009) and BOB (2011) results may be due to the acoustic imprint of the multibeam echosounder, which is much larger than the target size or to artifacts in the multibeam data related to secondary lobes, which would image the same gas flare on consecutive pings along the ship track. On the polar echogram in Fig. 10, a very clear gas flare is observed at the vertical of the OBS, together with some other gas flares of lesser amplitudes,

supporting the idea that the secondary lobes effects are quite important.

The BOB data provide additional information about the precise location of gas flares compared to the multibeam data.

The great advantage of BOB is the quantification of gas flow rates, for gas sources located entirely within a given sector, thanks to its calibrated split beam echosounder. However with its present configuration, BOB offers a very small study area with respect to the one imaged by the multibeam echosounder.

Interpreting non-seismic, short duration signals recorded on OBSs

The OBSs deployed within the Marmara Sea have recorded earthquakes, but also unconventional, non-seismic, micro-events (Tary et al. 2012) hereafter called “short duration events” (SDE). SDEs are commonly found on OBS records, in a variety of geological environments (Buskirk et al. 1981; Diaz et al. 2007). Because SDEs are very short in duration and they are not observed at more than one single OBS, they are not detected by automatic procedures used for locating micro-earthquakes, which usually require the identification of first arrivals on at least 3 distant stations. Hence, SDEs have for long remained undetected or simply disregarded, because considered as noise. Tary et al. (2012) have shown that SDEs from the Marmara seafloor differ from conventional micro-earthquakes by several aspects: (1) the duration of each SDE is less than 300–400 ms, (2) SDEs have a monochromatic frequency

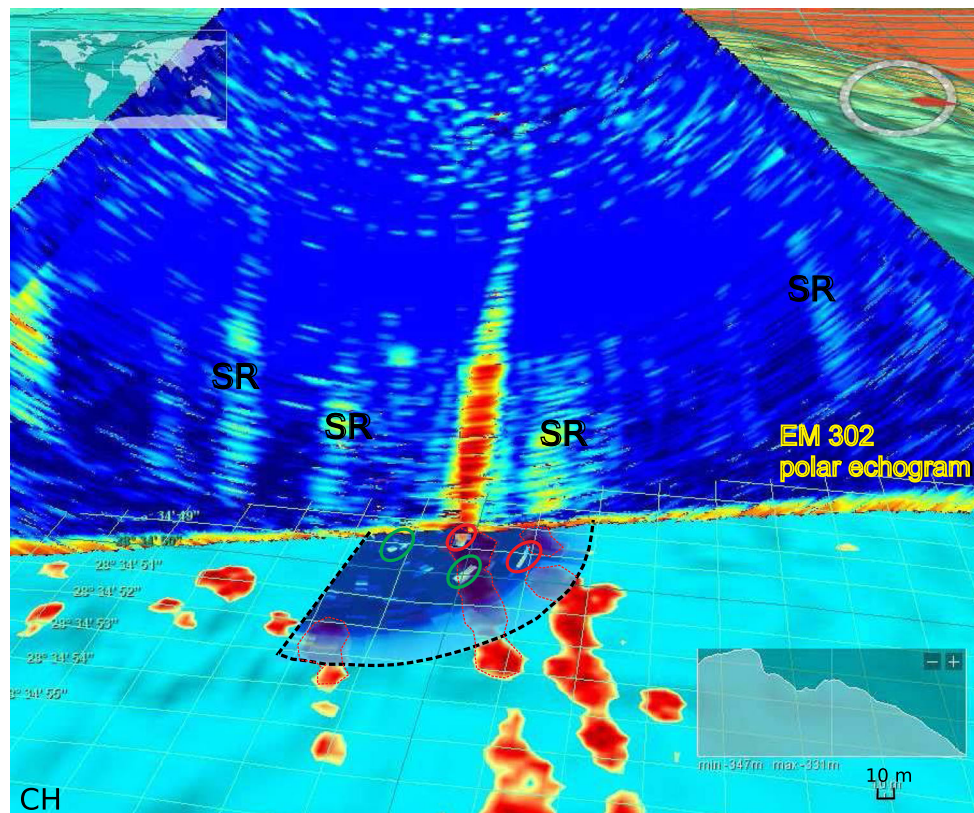


Fig. 10 Mosaic view of echo-integration results from EM302 and BOB focus on the Central High where BOB was deployed in 2011, with the EM302 polar echogram of the ping corresponding to the gas

bubble source beneath the OBS 04 location, imaged in 2009. Natural gas sources are surrounded in *green*. Echoes from OBS 04 and KATERINA are surrounded in *red*

content ranging between 10 and 30 Hz, (3) SDEs peak amplitudes are highly variable, comprised between 0.5 and 20 $\mu\text{m/s}$, (4) short durations of SDEs don't allow a clear identification of secondary arrivals such as S body waves or surface waves, 5) SDEs are detected by all geophone components (x, y, z); only those micro-events that have the largest amplitudes are detected on the hydrophone (Fig. 11). Based on the observations of the presence of gas in superficial sediments (in situ observations, chirp data) and on analogies with laboratory experiments, Tary et al. (2012) proposed that SDEs could be produced by the collapse of fluid-filled conduits induced by gas migration throughout superficial layers.

Figure 12 shows the SDE distribution near OBS 04, which was deployed in 2011 on the top of the Central High. The identification of SDE's was done automatically with a STA/LTA based code, and the picking was validated manually (i.e. trough visual observation). The OBS started recording on 15th at 15:00 pm, while acoustic data were collected only from April 12th to April 19th, 2011. Simultaneous recordings of seismologic and acoustic data over the 10th sector (where OBS04 is located) were efficient only during cycles 4 and 6 (no acoustic data from the

10th sector were collected during cycles 5 and 7). In addition, since the suggested natural gas emission source beneath the OBS may spread over several sectors, the acoustic data could not be compared to the seismologic data.

During the three months and half recording period, the number of SDEs recorded by OBS04 was nearly twice higher than the average SDE number calculated over 9 OBSs of the network, supporting the hypothesis that the OBS is located on a gas bubble and that the SDE's have a gas related origin (results from 9 OBSs are not shown here but available on request). The observed SDE activity might be related to the gas emission induced by the weight of the freshly deployed OBS. However, no decrease in activity that could be related to a return to equilibrium after the OBS deployment has been observed (Fig. 12).

On seismic sections, the leakage-related anomalies appear usually as lateral variations along reflections, as local increases or reductions in amplitude strength, continuity, frequency and/or AVO (amplitude versus offset) (e. g. Løseth et al. 2009). Figure 13 shows a W-E oriented chirp (1.8–5.3 kHz) profile acquired during the 2009 Marmesonet expedition across the Central High, 40 m

Fig. 11 An example of SDE imaged on the OBS 04 deployed in the Central High. *Top to bottom*, the two horizontal components, the vertical component and the hydrophone. *Right hand side* are the corresponding frequency spectra

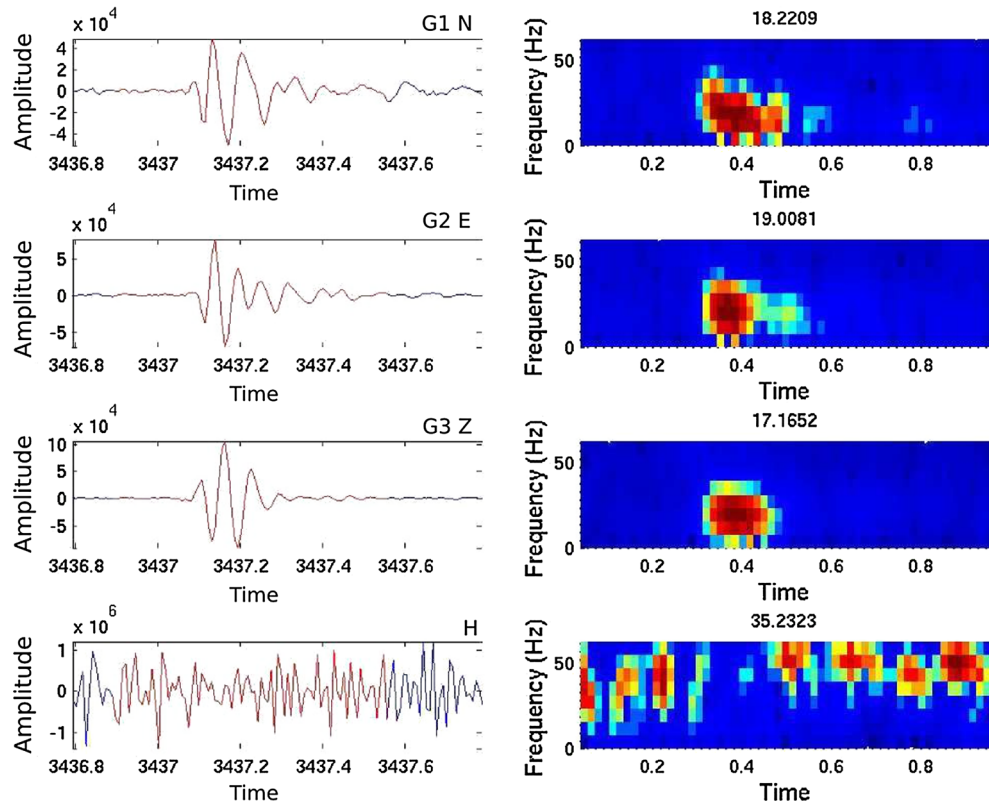
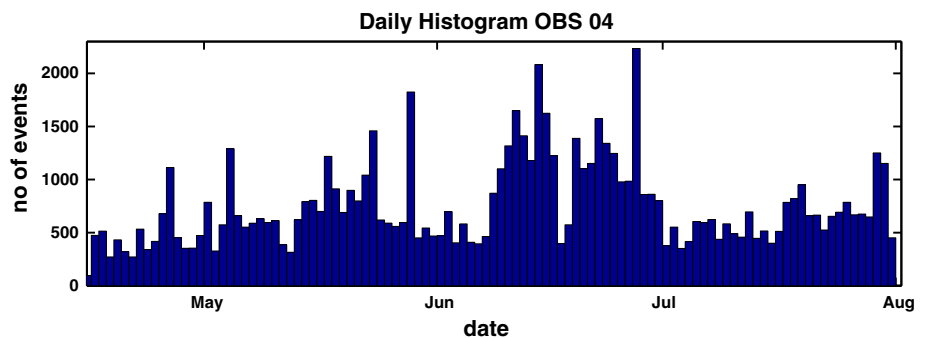


Fig. 12 Daily micro-event distribution on the OBS 04 of the Marmara 2011 network. More than 80,000 SDE's were identified on OBS 04 between April 15th and July 31st 2011



north of the BOB module (Fig. 1c). A strong amplitude reflection zone, roughly 8-10 m below the seabed is clearly visible exhibiting discontinuities and lateral amplitude variations. This enhanced reflection zone, identified along numerous Chirp profiles at the Central High and elsewhere in the Sea of Marmara, are systematically associated in the water column with acoustic gas flares (ship-borne EM302 records), and therefore are attributed to the presence of gas-saturated sediments. Where this level stops laterally (see western and eastern edges of the profile in Fig. 13), no gas emissions occur. BOB was deployed in 2011 on top of the Central High above a wide zone where sub-surface sediments are saturated in gas (Chirp profiles) with numerous gas escapes though the seabed into the water column (EM302 records).

Conclusions

The acoustic data acquired with the BOB module in 2009 show that gas emissions can be continuous or transient with a variety of emission durations. The associated echo-integration per layer allows to locate the gas emission sites, and shows that the amplitude of gas emissions vary at different scales (minutes, hours, days).

Gas emission sites observed during the Marmesonet 2009 data are made of several smaller sources, which may be linked at depth, splitting into several fractures in the upper sedimentary layers, and influenced by variations in pore pressure. The gas emission pattern follows a NW-SE orientation that is consistent with the orientations of bathymetric features and faults, suggesting the existence of

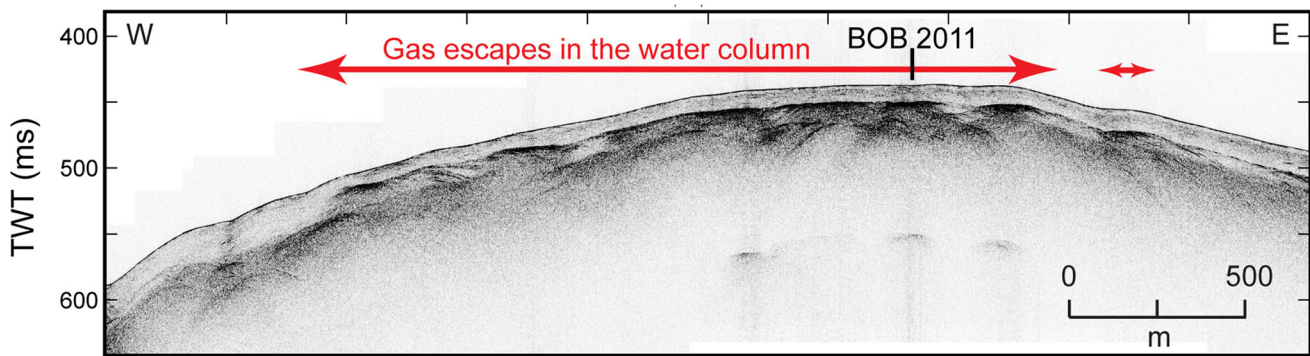


Fig. 13 W–E oriented chirp (1.8–5.3 kHz) profile acquired during the 2009 Marmesonet expedition across the Central High. Are reported the position of the BOB (deployed in 2011 and located 40 m south of this profile) and the wide zone, so-called “Istanbulle”, characterized by gas emissions in the water column recorded with

a low permeability zones of tectonic origin, such as fissure zones or footwalls of bathymetric relief.

Based on the acoustic data collected in 2011, two continuous gas bubble sources were identified, on the Central High. Volumetric flow rates ranging between 2 and 16 milliliters per minute are estimated. However, gas emission sources show spatial and temporal variations that are not necessarily related to variations in gas flow rates, but possibly to the dispersion of gas bubbles on neighboring sectors due to the sea-bottom currents. Such deviations should be more easily observable at layers near the BOB module where the insonified volume is smaller and when the source is located at the extremity of the insonified areas. This hypothesis may be easily checked by adding a three dimensional current-meter to the BOB module for future deployments.

The present study shows that the computed flow rates could be underestimated, if all gas bubbles emitted by the source are not located within the volume insonified by the 7° beam. It shows therefore the necessity to insonify continuously, but not sequentially like the present BOB configuration. Still, this option may also generate errors in the estimation of flow rates because bubbles would not occupy the totality of the insonified volume, which is a strong assumption for the echo-integration method (Foote 1983). The use of a multibeam echosounder, or several split beam echosounders may be possible solutions for insonifying continuously an area larger than 7°. However, the multibeam option does not offer the possibility to easily quantify gas flow rates, since the calibration of a multibeam echosounder is a meticulous issue without the split beam capacity to locate the target in three dimensions. Due to their small insonification volume, for geoscience applications a single splitbeam echosounder does not seem to have any advantage with respect to multibeam systems. Multiple

ship-borne multibeam echosounder during the same cruise (Dupré et al. 2010b). Gas bubbles in the water column are systematically associated in depth with strong amplitude reflectors (roughly 8–10 m below the seabed) attributed to the presence of gas in the sediments

split-beam echosounders option can be efficient solution, for the continuous monitoring and flow rate estimations.

Acoustic echoes reflected by OBS 04 do not appear as a fix and flat reflector. Instead, echoes are pixelated and have some spatial and temporal variations, suggesting that the OBS is located over a gas source. Gas flares mapped in 2009 with the ship-board multibeam echosounder EM302 over the Central High show also a gas emission pattern comprising the location of OBS 04, which more than 80,000 short duration events (SDEs) during a period of 3.5 months. The high amplitude reflector observed on the sub-bottom profiler data confirms the presence of gas within the sediments beneath OBS 04. This observation does strongly support, but does not provide undisputable proof, the hypothesis that the SDE's are gas related events (Tary et al. 2012).

Acknowledgments The data used in this paper was collected within the MARMARA-DM Demonstration mission of the ESONET (European Seas Observatory NETWORK) NoE supported by the 7th Framework Programme (FP7) of the EU. The specific study on BOB results presented here was funded by TOTAL. The Istanbul Technical University (ITU) provided long-term, valuable support for the operations at sea in 2009, and R/V Yunus for the deployment and recovery of BOB in 2011. The Turkish Navy provided special assistance that largely contributed to the success of the Marmesonet cruise of R/V Le Suroît in 2009 in the Sea of Marmara. Special acknowledgement to: Captain and crew of IFREMER/GENAVIR of R/V Le Suroît for their efforts during the Marmesonet cruise; Ronan Apprioual and Pascal Pelleau (IFREMER); Roger Galou (Altran); Namik Cagatay (ITU) and Pierre Henry (Cerege). Careful reviews by the two anonymous reviewers resulted in considerable improvement to an earlier version of this manuscript. We are particularly indebted to Jens Greinert, the reviewers and to the editor for their judicious insightful remarks.

References

- Alpar B (1999) Underwater signatures of the Kocaeli earthquake of 17 August 1999 in Turkey. *Turk J Mar Sci* 5:111–130

- Alpar B, Yuce H (1997) Short and tidal period sea-level variations along the Turkish Strait system. *Turk J Mar Sci* 3:11–22
- Armijo R, Pondard N, Meyer B, Uçarkus G (2005) Submarine fault scarps in the Sea of Marmara pull-apart (North Anatolian Fault): implications for seismic hazard in Istanbul. *Geochem Geophys Geosyst* 6:Q06009
- Artemov YG, Egorov VN, Polikarpov GG, Gulin SB (2007) Methane emission to the hydro—and atmosphere by gas bubble streams in the Dnieper paleo-delta, the Black Sea (in Russian). *Rep Natl Acad Sci Ukr* 5:110–116
- Bayon G, Dupré S, Ponzevera E, Etoubleau J, Cheron S, Pierre C, Mascle J, Boetius A, de Lange GJ (2013) Formation of carbonate chimneys in the Mediterranean Sea linked to deep-water oxygen depletion. *Nat Geosci* 6 (9):755–760. doi:10.1038/ngeo1888. <http://www.nature.com/ngeo/journal/v6/n9/abs/ngeo1888.html#supplementary-information>
- Boetius A, Ravensschlag K, Schubert CJ, Rickert D, Widdel F, Gieseke A, Amann R, Jorgensen BB, Witte U, Pfannkuche O (2000) A marine microbial consortium apparently mediating anaerobic oxidation of methane. *Nature* 407(6804):623–626
- Boles JR, Clark JF, Leifer I, Washburn L (2001) Temporal variation in natural methane seep rate due to tides, Coal Oil point area, California. *J Geophys Res* 106(11):27077–27086
- Bourry C, Chazallon B, Charlou JL, Donval JP, Ruffine L, Henry P, Géli L, Çagatay N, Inan S, Moreau M (2009) Free gas and gas hydrates from the Sea of Marmara, Turkey Chemical and structural characterization. *Chem Geol* 264:197–206
- Briggs KB, Richardson MD (1996) Variability in in situ shear strength of gassy muds. *Geo Mar Lett* 16:189–195
- Buskirk RE, Frohlich C, Latham GV, Chen AT, Lawton J (1981) Evidence that biological activity affects ocean bottom seismograph recordings. *Mar Geophys Res* 5(2):189–205
- Clift R, Grace JR, Weber ME (1978) Bubbles, drops, and particles 380. Academic Press, New York
- Crémière A, Bayon G, Ponzevera E, Pierre C (2013) Paleo-environmental controls on cold seep carbonate authigenesis in the Sea of Marmara. *Earth Planet Sci Lett* 376:200–211. doi:10.1016/j.epsl.2013.06.029
- Diaz J, Gallart J, Gaspà O (2007) Atypical seismic signals at the Galicia Margin, North Atlantic Ocean, related to the resonance of subsurface fluid-filled cracks. *Tectonophysics* 433:1–13. doi:10.1016/j.tecto.2007.01.004
- Dragesund O, Olsen S (1965) On the possibility of estimating year-class strength by measuring echo-abundance of 0-group fish. *Fiskeridirektoratets Skrifter Serie Havundersøkelser* 13(8):48–65
- Duan Z, Møller N, Weare JH (1992a) An equation of state for the CH₄–CO₂–H₂O system: I. Pure systems from 0–1,000°C and 0 to 8,000 bar. *Geochim Cosmochim Acta* 56:2605–2617
- Duan Z, Møller N, Weare JH (1992b) An equation of state for the CH₄–CO₂–H₂O system: II. Mixtures from 50–1,000 & #xB0;C and 0 to 1,000 bar. *Geochim Cosmochim Acta* 56:2619–2631
- Dupré S, Buffet G, Mascle J, Foucher J-P, Gauger S, Boetius A, Marfia C, the AsterX AUV Team, the Quest ROV Team, the BIONIL Scientific Party (2008) High-resolution mapping of large gas emitting mud volcanoes on the Egyptian continental margin (Nile Deep Sea Fan) by AUV surveys. *Mar Geophys Res* 29(4):275–290. doi:10.1007/s11001-009-9063-3
- Dupré S, Woodside J, Klaucke I, Mascle J, Foucher J-P (2010a) Widespread active seepage activity on the Nile Deep Sea Fan (offshore Egypt) revealed by high-definition geophysical imagery. *Mar Geol* 275(1–4):1–19
- Dupré S, Scalabrin C, Géli L, Henry P, Grall C, Tary J-B, Çagatay MN, Imren C, The MARMESONET Scientific Party Team (2010b) Widespread gas emissions in the Sea of Marmara in relation with the tectonic and sedimentary environments: results from shipborne multibeam echosounder water column imagery (MARMESONET expedition, 2009). *Eur Geosci Union Gen Assem* 12:9429
- Ergin M, Saydam C, Baştürk Ö, Erdem E, Yörük R (1991) Heavy metal concentrations in surface sediments from the two coastal inlets (Golden Horn Estuary and Izmit Bay) of the northeastern sea of Marmara. *Chem Geol* 91:269–285
- Fischer PJ (ed) (1978) Natural gas and oil seeps, Santa Barbara Basin, California. In: California offshore gas, oil, and tar seeps. California State Lands Commission, Sacramento, California, pp 1–62
- Foote KG (1982) Optimizing copper spheres for precision calibration of hydroacoustic equipment. *J Acoust Soc Am* 71:742–747
- Foote KG (1983) Use of elastic spheres as calibration targets. In: Nakken O, Venema SC (eds) Symposium on Fisheries Acoustics. FAO Fisheries Report No. 300, pp 52–58
- Foote KG, Knudsen HP, Vestnes G, MacLennan DN, Sirnmonds EJ (1987) Calibration of acoustic instruments for fish density estimation: a practical guide. *ICES Coop Res Rep* 144:69
- Foucher JP, Dupré S, Scalabrin C, Feseker T, Harmegnies F, Nouzé H (2010) Changes in seabed morphology, mud temperature and free gas venting at the Håkon Mosby Mud Volcano, offshore Northern Norway, over the time period 2003–2006. *Geo Mar Lett* 30:157–167
- Gasparini L, Polonia A, Del Bianco F, Etiope G, Marinario G, Favali P, Italiano F, Çagatay MN (2012) Gas seepages and seismogenic structures along the North Anatolian Fault in the eastern Marmara Sea. *Geochem Geophys Geosyst* 13:Q10018. doi:10.1029/2012GC004190
- Géli L, Henry P, Zitter T, Dupré S, Tryon M, Çagatay NM, Mercier de Lépinay B, Le Pichon X, Sengör AMC, Görür N, Natalin B, Uçarkus G, Özeren S, Volker D, Gasparini L, Bourlange S, The Marnaut Scientific Party (2008) Gas emissions and active tectonics within the submerged section of the North Anatolian Fault zone in the Sea of Marmara. *Earth Planet Sci Lett* 274:34–39
- Géli L, Henry P, Çagatay N (2009) Report of Marmesonet Cruise of R/V Le Suroit, Leg 1 (November 4–25, 2009). p.f.henry.free.fr/marmara/public/MARMESONET/Marmesonet_Leg1_Cruise_Report_FINAL.pdf
- Grall C, Henry P, Tezcan D, Géli L, de Lépinay BM, Rudkiewicz L-J, Zitter T, Harmegnies F (2012) Heat flow in the Sea of Marmara Central Basin: possible implications for the tectonic evolution of the North Anatolian Fault. *Geology* 40:3–6. doi:10.1130/G32192.1
- Greiner J (2008) Monitoring temporal variability of bubble release at seeps: the hydroacoustic swath system GasQuant. *J Geophys Res Oceans* 113:20
- Greiner J, Nutz B (2004) Hydroacoustic experiments to establish a method for the determination of methane bubble fluxes at cold seeps. *Geo Mar Lett* 24:75–85. doi:10.1007/s00367-003-0165-7
- Greiner J, Artemov Y, Egorov V, De Batist M, McGinnis D (2006) 1300-m-high rising bubbles from mud volcanoes at 2080 m in the Black Sea: hydroacoustic characteristics and temporal variability. *Earth Planet Sci Lett* 244(1–2):1–15. doi:10.1016/j.epsl.2006.02.011
- Henry P, and MarNaut Cruise Sci. Party (2007) MarNaut Cruise of R/V L'Atalante report (2007). p.f.henry.free.fr/marmara/marnaut_public/marnaut_final_reports/MARNAUT_report.pdf
- Hornafius JS, Derek Q, Luyendyk BP (1999) The world's most spectacular marine hydrocarbon seeps (Coal Oil Point, Santa Barbara Channel, California): quantification of emissions. *J Geophys Res* 104:20703–20712. doi:10.1029/1999JC900148
- Hovland M (2007) Discovery of prolific natural methane seeps at Gullfaks, northern North Sea. *Geo Mar Lett* 27(2–4):197–201
- Hovland M, Sommerville JH (1985) Characteristics of two natural gas seepages in the North Sea. *Mar Pet Geol* 2:319–326

- Hustoft S, Bünz S, Mienert J, Chand S (2009) Gas hydrate reservoir and active methane-venting province in sediments on <20 Ma young oceanic crust in the Fram Strait, offshore NW-Svalbard. *Earth Planet Sci Lett*. doi:[10.1016/j.epsl.2009.03.038](https://doi.org/10.1016/j.epsl.2009.03.038)
- Judd A, Hovland M (2007) Seabed fluid flow: the impact on geology, biology and the marine environment. Cambridge University Press, Cambridge 475
- Knies J, Damm E, Gutt J, Mann U, Pinturier L (2004) Near-surface hydrocarbon anomalies in shelf sediments off Spitsbergen: evidences for past seepages. *Geochem Geophys Geosyst* 5:Q06003. doi:[10.1029/2003GC000687](https://doi.org/10.1029/2003GC000687)
- Kopf A, Delisle G, Faber E, Panahi B, Aliyev CS, Guliyev I (2009) Long-term in situ monitoring at Dashgil mud volcano, Azerbaijan: a link between seismicity, pore-pressure transients and methane emission. *Int J Earth Sci* 99:227–240 and Erratum 99: 241
- Kopf A, Delisle G, Faber E, Panahi B, Aliyev CS, Guliyev I (2010) Long-term in situ monitoring at Dashgil mud volcano, Azerbaijan: a link between seismicity, pore-pressure transients and methane emission. *Int J Earth Sci* 99:227–240. doi:[10.1007/s00531-009-0487-4](https://doi.org/10.1007/s00531-009-0487-4)
- Kuşçu İ, Okamura M, Matsuoka H, Awata Y (2002) Active faults in the Gulf of İzmit on the North Anatolian Fault, NW Turkey: a high-resolution shallow seismic study. *Mar Geol* 190:421–443
- Kuscu I, Okamura M, Matsuoka H, Gokasan E, Awata Y, Tur H, Simsek M (2005) Seafloor gas seeps and sediment failures triggered by the August 17, 1999 earthquake in the Eastern Part of the Gulf of İzmit, Sea of Marmara, NW Turkey. *Mar Geol* 215:193–214
- Laigle M, Bécel A, de Voogd B, Hirn A, Taymaz A, Ozalaybey S, Members of SEISMARMARA Leg 1 Team (2008) A first deep seismic survey in the Sea of Marmara: deep basins and the whole crust architecture and evolution. *Earth Planet Sci Lett* 270:168–179. doi:[10.1016/j.epsl.2008.02.031](https://doi.org/10.1016/j.epsl.2008.02.031)
- Le Pichon X, Sengor AMC, Demirbag E, Rangin C, Imren C, Armijo R, Gorur N, Cagatay N, Mercier de Lépinay B, Meyer B, Saatçilar R, Tok B (2001) The active Main Marmara fault. *Earth Planet Sci Lett* 192:595–616
- Leblond I, Scalabrin C, Berger L (2014) Acoustic monitoring of gas emissions from the seafloor. Part I: quantifying the volumetric flow of bubbles. *Mar Geophys Res* (this issue). doi:[10.1007/s11001-014-9223-y](https://doi.org/10.1007/s11001-014-9223-y)
- Leifer JR, Boles BP (2005a) Measurement of marine hydrocarbon seep flow through fractured rock and unconsolidated sediment. *Mar Pet Geol* 22:551–568. doi:[10.1016/j.marpetgeo.2004.10.026](https://doi.org/10.1016/j.marpetgeo.2004.10.026)
- Leifer I, Boles JR (2005b) Turbine tent measurements of marine hydrocarbon seeps on subhourly timescales. *J Geophys Res* 110:C01006. doi:[10.1029/2003JC002207](https://doi.org/10.1029/2003JC002207)
- Leifer I, Clark JF (2002) Modeling trace gases in hydrocarbon seep bubbles: application to marine hydrocarbon seeps in the Santa Barbara Channel. *Russ Geol Geophys* 47:572–579
- Leifer I, Boles JR, Luyendyk BP, Clark JF (2004) Transient discharges from marine hydrocarbon seeps: spatial and temporal variability. *Environ Geol Berl* 46:1038–1052. doi:[10.1007/s00254-004-1091-3](https://doi.org/10.1007/s00254-004-1091-3)
- Leighton TG, White PR (2011) Quantification of undersea gas leaks from carbon capture and storage facilities, from pipelines and from methane seeps, by their acoustic emissions. *Proc R Soc A Math Phys Eng Sci* 468(2138):485–510
- Limonov AF, van Weering TCE, Kenyon NH, Ivanov MK, Meisner LB (1997) Seabed morphology and gas venting in the Black Sea mudvolcano area: observations with the MAK-1 deep-tow sidescan sonar and bottom profiler. *Mar Geol* 137:121–136
- Løseth H, Gading M, Wensaas L (2009) Hydrocarbon leakage interpreted on seismic data. *Mar Pet Geol* 26:1304–1319
- Mattson MD, Likens GE (1990) Air pressure and methane fluxes. *Nature* 347:718–719. doi:[10.1038/347718b0](https://doi.org/10.1038/347718b0)
- Mau S, Rehder G, Arroyo IG, Gossler J, Suess E (2007) Indications of a link between seismotectonics and CH₄ release from seeps off Costa Rica. *Geochem Geophys Geosyst* 8:1–13
- Medwin H, Clay SC (1998) Fundamentals of acoustical oceanography. Academic Press, San Diego, p 712
- Merewether R, Olsson MS, Lonsdale P (1985) Acoustically detected hydrocarbon plumes rising from 2-km Depths in Guaymas Basin, Gulf of California. *J Geophys Res* 90:3075–3085. doi:[10.1029/JB090iB04p03075](https://doi.org/10.1029/JB090iB04p03075)
- Mienert J, Bünz S, Guidard S, Vanneste M, Berndt C (2005) Ocean bottom seismometer investigations in the Ormen Lange area offshore mid-Norway provide evidence for shallow gas layers in subsurface sediments. *Mar Pet Geol* 22(1–2):287–297. doi:[10.1016/j.marpetgeo.2004.10.020](https://doi.org/10.1016/j.marpetgeo.2004.10.020)
- Nikolovska A, Sahling H, Bohrmann G (2008) Hydroacoustic methodology for detection, localization, and quantification of gas bubbles rising from the seafloor at gas seeps from the eastern Black Sea. *Geochem Geophys Geosyst* 9(10). doi:[10.1029/2008GC002118](https://doi.org/10.1029/2008GC002118)
- Obzhairov A, Shakirov R, Salyuk A, Suess E, Biebow M, Salomatin A (2004) Relations between methane venting, geological structure and seismo-tectonics in the Okhotsk Sea. *Geo Mar Lett* 24:135–139
- Ostrovsky I, McGinnis D, Lapidus L, Eckert W (2008) Quantifying gas ebullition with echosounder: the role of methane transport by bubbles in a medium-sized lake. *Limnol Oceanogr Methods* 6:105–118
- Rangin C, Demirbag E, Imren C, Crusson A, Normand A, Le Drezen E, Le Bot A (2001) Marine atlas of the Sea of Marmara (Turkey). Ifremer, Plouzané. ISBN 2-84433-068-1
- Sauter EJ, Muyakshin SI, Charlou J-L, Schluter M, Boetius A, Jerosch K, Damm E, Foucher J-P, Klages M (2006) Methane discharge from a deep-sea submarine mud volcano into the upper water column by gas hydrate-coated methane bubbles. *Earth Planet Sci Lett* 243:354–365
- Schneider von Deimling JS, Brockhoff J, Greinert J (2007) Flare imaging with multibeam systems: data processing for bubble detection at seeps. *Geochem Geophys Geosyst* 8(6). doi:[10.1029/2007GC001577](https://doi.org/10.1029/2007GC001577)
- Schneider von Deimling J, Papenberg C (2012) Technical note: detection of gas bubble leakage via correlation of water column multibeam images. *Ocean Sci* 8(2):175–181
- Schneider von Deimling J, Greinert J, Chapman NR, Rabbel W, Linke P (2010) Acoustic imaging of natural gas seepage in the North Sea: sensing bubbles controlled by variable currents. *Limnol Oceanogr Methods* 8:155–171
- Schneider von Deimling J, Rehder G, Greinert J, McGinnis DF, Boetius A, Linke P (2011) Quantification of seep-related methane gas emissions at Tommeliten, North Sea. *Cont Shelf Res* 31:867–878
- Şengör AMC, Tüysüz O, Imren C, Sakiç M, Eydoğan H, Görür N, Le Pichon X, Rangin C (2005) The North Anatolian Fault: a New Look. *Annu Rev Earth Planet Sci* 33:37–112. doi:[10.1146/annurev.earth.32.101802.120415](https://doi.org/10.1146/annurev.earth.32.101802.120415)
- Sills GC, Wheelers SJ, Thomas SD, Gardner ND (1991) The behaviour of offshore soils containing gas bubble. *Geotechnique* 41:227–242
- Simmonds J, MacLennan DN (2005) Fisheries Acoustics. Blackwell Publishing, London
- Stanton TK (1989) Simple approximate formulas for backscattering of sound by spherical and elongated objects. *J Acoust Soc Am* 86(4):1499
- Tary J-B (2011) Relations entre fluides et sismicité dans le domaine sous-marin à partir de sismographes de fond de mer : étude de cas en Mer de Marmara et Application au Delta du Niger. PhD theseis, Ifremer, Brest

- Tary J-B, Géli L, Guennou G, Henry P, Sultan N, Cagatay N, Vidal V (2012) Microevents produced by gas migration and expulsion at the seabed: a study based on sea bottom recordings from the Sea of Marmara. *Geophys J Int.* doi:[10.1111/j.1365-246X.2012.05533.x](https://doi.org/10.1111/j.1365-246X.2012.05533.x)
- Tryon MD, Brown KM, Torres ME (2002) Fluid and chemical flux in and out of the sediments, hosting methane hydrate deposits on Hydrate Ridge, OR, II: hydrological processes. *Earth Planet Sci Lett* 201:541–557
- Westbrook G K et al (2009) Escape of methane gas from the seabed along the West Spitsbergen continental margin. *Geophys Res Lett.* doi:[10.1029/2009GL039191](https://doi.org/10.1029/2009GL039191)
- Westbrook GK, Chand S, Rossi G, Long C, Büinz S, Camerlenghi A, Carcione JM, Dean S, Foucher J-P, Flueh ER, Gei D, Hacke R, Madrussani G, Mienert J, Minshull TA, Nouzé H, Peacock S, Reston TJ, Vanneste M, Zillmer M (2008) Estimation of hydrate concentration from multi-component seismic data at sites in the continental margins of NW Svalbard and the Storegga region of Norway. *Mar Pet Geol* 25:744–758
- Wever TF, Lühder R, Voß H, Knispel U (2006) Potential environmental control of free shallow gas in the seafloor of Eckernförde Bay, Germany. *Mar Geol* 225:1–4. doi:[10.1016/j.margeo.2005.08.005](https://doi.org/10.1016/j.margeo.2005.08.005)
- Wheeler SJ, Gardiner TN (1989) Elastic moduli of soils containing large gas bubbles. *Geotechnique* 39(2):333–342
- Yüce H (1993) Analysis of the water level variations in the Eastern Black Sea. *J Coast Res* 9(4):1075–1082
- Zitter TAC, Henry P, Aloisi G, Delaygue G, Çagatay MN, Mercier de Lepinay B, Al-Samir M, Fornacciari F, Tesmer M, Pekdeger A, Wallmann K, Lericolais G (2008) Cold seeps along the main Marmara Fault in the Sea of Marmara (Turkey). *Deep Sea Res Part I* 55:552